JACS Au
AN OPEN ACCESS JOURNAL OF THE AMERICAN CHEMICAL SOCIETY

pubs.acs.org/jacsau

Article

Suppressing the Excitonic Effect in Covalent Organic Frameworks for Metal-Free Hydrogen Generation

Hongde Yu and Dong Wang*

Cite This: *JACS Au* 2022, 2, 1848−1856

Read Online

ACCESS | Metrics & More | Article Recommendations | Supporting Information

ABSTRACT: Photocatalytic hydrogen generation is a promising solution for renewable energy production and plays a role in achieving carbon neutrality. Covalent organic frameworks (COFs) with highly designable backbones and inherent pores have emerged as novel photocatalysts, yet the strong excitonic effect in COFs can impede the promotion of energy conversion efficiency. Here, we propose a facile approach to suppress the excitonic effect in COFs, which is by narrowing the band gap and increasing the dielectric screening via a rational backbone design and chemical modifications. Based on the GW-BSE method, we uncover a linear relationship between the electronic dielectric constant and the inverse square of the optical band gap of COFs of the Lieb lattice. We further demonstrate that both reduced exciton binding energy and enhanced sunlight absorption can be simultaneously realized in COFs with a narrow band gap. Specifically, we show that one of our designed COFs whose exciton binding energy is nearly half that of g-C_3N_4 is capable of metal-free hydrogen production under near-infrared light irradiation. Our results showcase an effective method to suppress the excitonic effect in COFs and also pave the way for their applications in photocatalytic, photovoltaic, and other related solar energy conversions.

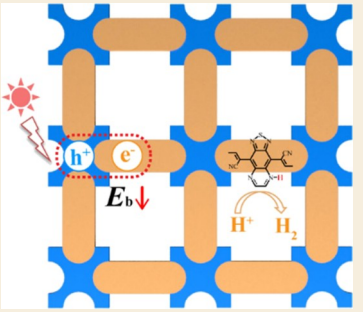

KEYWORDS: *excitonic effect, organic photocatalysts, hydrogen evolution reaction, covalent organic frameworks*

INTRODUCTION

Photocatalytic hydrogen generation is a potential approach to utilize inexhaustible sunlight and earth-abundant water for hydrogen fuel production, which has become one of the clean and sustainable solutions to the global energy crisis.[1−4] Since the first demonstration of a TiO_2 photoanode and a Pt counterelectrode for water oxidation and reduction in the 1970s,[5] solar-to-hydrogen (STH) energy conversion has attracted tremendous attention.[6,7] Inspired by natural photosynthesis, organic semiconductors with tunable electronic structures, represented by g-C_3N_4,[8,9] conjugated microporous polymers,[10] linear conjugated polymers,[11−13] two-dimensional (2D) polymers,[14−16] and covalent organic frameworks (COFs),[17−24] have emerged as novel photocatalysts. COFs are a class of porous materials where the molecular building blocks are integrated into periodic skeletons via reticular chemical reactions.[25,26] The unique attributes of COFs including high crystallinity, a tunable pore size, a large specific surface area, and high chemical and thermal stability make them promising candidates for photocatalysis.[27−32] Very recently, layer-stacked COFs with impressive hydrogen evolution activities have been reported, such as azine-linked N_3-COF and cyano-vinylene-linked sp^2c-COF, and it was shown that functionalization of sp^2c-COF with electron-withdrawing end groups further increased the hydrogen production rate.[18,22] Despite the rapid experimental progress,[33−40] few studies reported an STH energy conversion efficiency of above 1%.[9] Therefore, molecular insight and subtle regulation of the determining factors in photoelectrochemical conversions, including solar light harvest, exciton dissociation, charge carrier transport, and redox reaction overpotentials, are highly demanded in order to achieve more efficient hydrogen production.[33]

Among these factors, the excitonic effect in organic photocatalysts has been drawing intense attention.[41−44] Due to the small dielectric constant (ε_s) of organic materials, the photoexcited electron−hole pair, namely, the exciton, is strongly bounded, which will hamper its dissociation into free charge carriers and foster undesirable exciton decay.[43] Although the behavior of excitons in several COFs has been reported, such as porphyrin-based COFs (DhaTph-M) and COF-5,[41,42] a general approach to regulate the excitonic effect is lacking, which calls for fundamental understanding of the structure−property relationship in COFs. The excitonic effect and optical absorption are inter-related properties of excitons, and both of them show a significant influence on the photocatalytic performance of COFs. Thereby, the goal of our study is to unravel their relations and demonstrate how to

Received: March 15, 2022
Revised: June 5, 2022
Accepted: June 8, 2022
Published: June 22, 2022

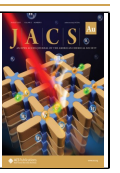

https://doi.org/10.1021/jacsau.2c00169
JACS Au 2022, 2, 1848−1856

suppress the excitonic effect by tailoring the chemical building blocks of COFs.

In this study, by exploring the interplay of optical band gap, exciton binding energy, and chemical structure of COFs, we present a robust approach to regulate the excitonic effect in these organic photocatalysts for efficient hydrogen generation. We design a series of fully conjugated COFs of the Lieb lattice that can be synthesized via the Knoevenagel polycondensation reaction. By choosing appropriate molecular building blocks and chemical modifications, we are able to tune their band gaps from 1.72 to 1.00 eV to harvest the visible and near-infrared (NIR) light. More importantly, with the state-of-the-art GW-BSE method, we unravel a positive correlation between the exciton binding energy and the optical band gap. These findings indicate that narrowing the band gap of COFs not only enhances the sunlight absorption in the visible and NIR region, which accounts for about 80% of energy in the solar spectrum, but also profits the exciton dissociation and utilization to boost the energy conversion efficiency. Finally, we demonstrate that one of the newly designed COFs whose exciton binding energy is only half that of g-C_3N_4, a typical organic photocatalyst, is capable of photocatalytic hydrogen production under the visible-to-NIR light irradiation with a high theoretical STH energy conversion efficiency. The established structure−property relationship will not only shed light on the rational design of new COFs with superior photocatalytic activity but also tremendously boost their applications in other solar energy conversion techniques.[45,46]

RESULTS AND DISCUSSION

Tuning the Band Gap of COFs To Harvest Visible and NIR Light

Although designing narrow band gap semiconductors for organic photovoltaics has shown great success in utilizing infrared photons and producing higher power conversion efficiencies,[47] it is unclear whether it is suitable for photocatalytic hydrogen evolution reaction (HER) due to the rigorous criterion for band alignments and driving force in chemical reactions. So far, most COFs used for photocatalysis possess wide band gaps, for example, 2.6−2.7 eV for N_x-COFs (x = 0−3),[18] 2.8 eV for TFPT-COF,[48] and 2.5 eV for BDT-ETTA COF.[19] Designing novel COFs with narrow band gaps and advanced photocatalytic activity is desired. COFs of the Lieb lattice are composed of two types of building blocks with a C_2 or C_4 symmetry, that is, nodes and edges. Such a construction offers tremendous opportunities to tune their electronic properties, especially the band gap and band edge energies, and explore their structure−property relationship for photocatalytic applications.[49−52]

In order to attain suitable band gaps and optimal band edge positions for the visible-to-NIR light-driven hydrogen production, we concurrently adopt two methods: (1) choosing edge building blocks with lower lowest unoccupied molecular orbital (LUMO) energy and (2) further modifying these building blocks with electron-withdrawing functional groups, which can be realized by a postsynthesis strategy. Based on these methods, we design a series of fully conjugated COFs with pyrene as a node, cyano-vinylene as a linkage, and various edge units. These COFs are denoted as PPy-Ph, PPy-BT, PPy-BT(F), PPy-PT, PPy-PT(F), PPy-TDQ, PPy-TzBI, PPy-Q, and PPy-Q(F), respectively, as illustrated in Figure 1. Herein, PPy represents the pyrene node and it is short for tetrakis(4-formylphenyl)phenyl; Ph, BT, PT, TDQ, TzBI, and Q represent the edges, which are short for phenyl, benzothiadiazole, pyridal[2,1,3]thiadiazole, thiadiazoloquinoxaline, pyrrolo-[3,4-f]benzotriazole-5,7-dione, and quinoxaline; F represents peripheral fluorine substitution. Among them, PPy-Ph is the so-called sp^{2}c-COF, which has been experimentally synthesized. Other COFs are constructed for the first time and they share the same Lieb lattice as sp^{2}c-COF. Furthermore, benefiting from the generality of the Knoevenagel polycondensation reaction,[46,53−55] these newly designed COFs may be synthesized with chemicals that have been widely used to fabricate organic photovoltaic polymers, as summarized in Figure S1.[35,45,56]

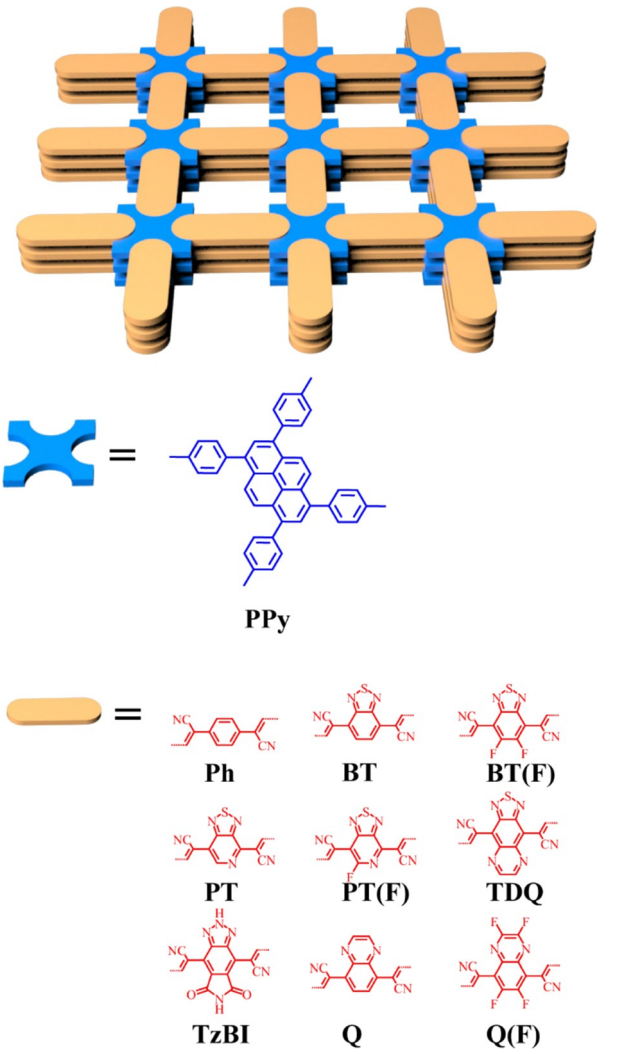

Figure 1. Topological structure and building blocks of stacked 2D COFs of the Lieb lattice with the nodes highlighted in blue and edges in orange. Chemical structures of node and edge units are shown below, including PPy, Ph, BT, BT(F), PT, PT(F), TDQ, TzBI, Q, and Q(F). PPy represents the pyrene-based node and it is short for tetrakis(4-formylphenyl)phenyl. Ph, BT, PT, TDQ, TzBI, and Q represent the edge, which are short for phenyl, benzothiadiazole, pyridal[2,1,3]thiadiazole, thiadiazolo-quinoxaline, pyrrolo[3,4-f]-benzotriazole-5,7-dione, and quinoxaline, respectively. F stands for fluorine substitution.

We calculate the band gap and band alignments of these COFs using the density functional theory (DFT), and we find that the band gap of COFs correlates positively with the

https://doi.org/10.1021/jacsau.2c00169
JACS Au 2022, 2, 1848−1856

LUMO energy of edges, which means that the lower the LUMO energy of edges, the smaller the band gap (Figures 2a,b, S2, and Table S1). Among them, PPy-Ph possesses the largest band gap. As reported by Jin and co-workers,[22] PPy-Ph exhibited highly active hydrogen production of about 2.1 mmol h^{-1} g^{-1} under visible light irradiation. Our calculations show that PPy-Ph is a semiconductor with an indirect band gap of 1.72 eV (Figure 2a, calculated by the HSE06 method), consistent with the experimental result of 1.9 eV.[22] Both conduction band minimum (CBM) and valence band maximum (VBM) of PPy-Ph are comprised of C-2p_z orbitals, confirming the formation of the extended π-conjugation.[57] As for band edge energies, VBM and CBM of PPy-Ph relative to the vacuum level are −5.24 and −3.52 eV, indicating its capability of photocatalytic HER, whereas it prohibits the oxygen evolution reaction (OER) (Figure 2a). Our results agree with the superior HER activity (2.1 mmol g^{-1} h^{-1}) and very small OER rate (0.022 mmol g^{-1} h^{-1}) of PPy-Ph observed in the experiment.[22]

All other COFs possess smaller band gaps than PPy-Ph (Table 1, Figures 2a, S3−S16, and Table S2). PPy-TDQ shows

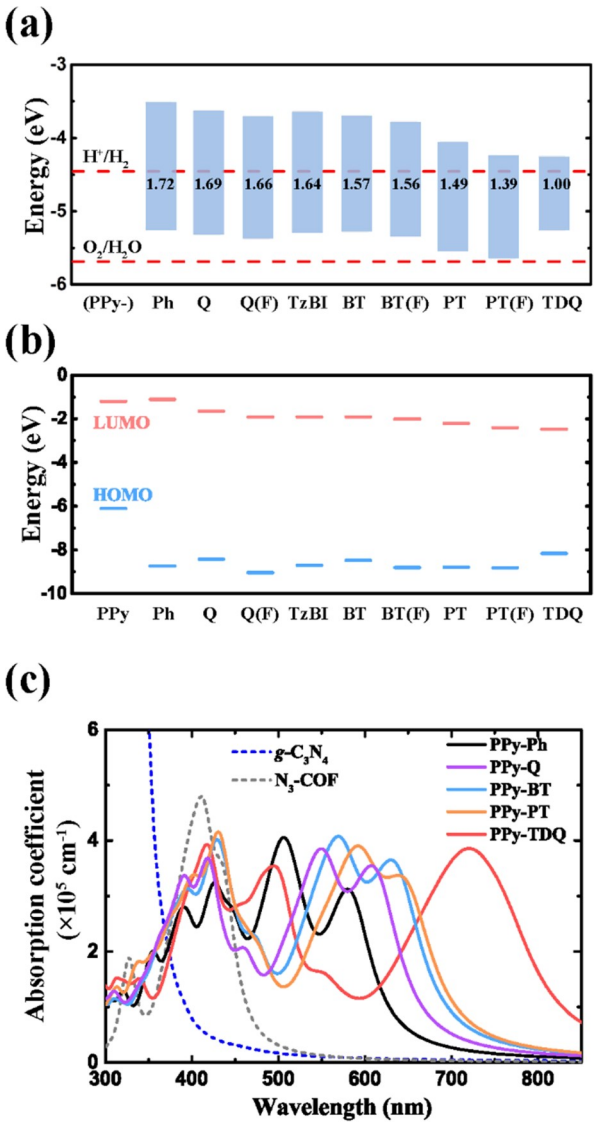

Figure 2. (a) Energies of VBM and CBM in COFs relative to the vacuum level calculated with the HSE06 functional. The red dashed lines represent the redox potentials of water at pH = 0. Band gaps of COFs are also shown in the figure. (b) HOMO and LUMO energy level diagram for molecular building blocks of COFs. PPy represents the pyrene node, and Ph, BT, BT(F), PT, PT(F), TDQ, TzBI, Q, and Q(F) represent edges of COFs. (c) Optical absorption spectra of PPy-Ph, PPy-BT, PPy-PT, PPy-TDQ, and PPy-Q in comparison to g-C_3N_4 and N_3-COF. All these spectra are calculated with the G_0W_0-BSE method.

Table 1. Quasi-Particle Optical Band Gap (E_{opt}) Calculated with the G_0W_0-BSE Method, Electric Band Gap (E_g) Calculated with the HSE06 Functional, Light-Induced Bias Potential of Electron (U), Reduced Mass of Exciton ($m^*_{exciton}$), Upper Limit of STH Energy Conversion Efficiency, Static Dielectric Constant (ε_s), and Exciton Binding Energy (E_b) of the Designed COFs

(PPy-)	E_{opt} (eV)	E_g (eV)	U (eV)	$m^*_{exciton}/m_e$	STH/%	ε_s	E_b (meV)
Ph	2.14	1.72	0.92	0.21	27.8	3.60	1200
Q	2.04	1.69	0.81	0.26	28.8	4.22	960
Q(F)	2.11	1.66	0.73	0.29	29.7	4.65	910
TzBI	2.06	1.64	0.81	0.34	30.4	4.02	1060
BT	1.96	1.57	0.73	0.19	32.8	4.50	940
BT(F)	2.03	1.56	0.67	0.25	33.1	4.00	1090
PT	1.94	1.49	0.40	0.27	35.6	4.63	920
PT(F)	1.88	1.39	0.18	0.25	39.5	5.12	900
TDQ	1.72	1.00	0.19	0.29	56.6	6.05	700

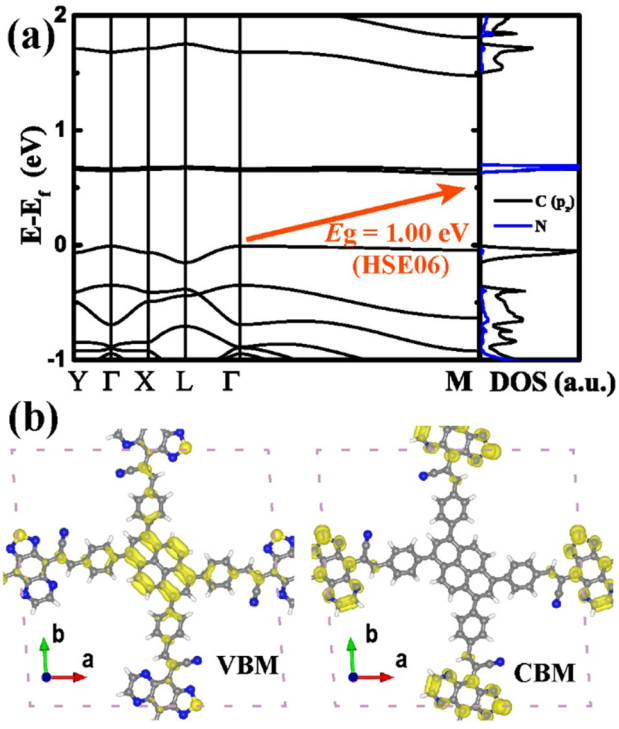

Figure 3. (a) Band structure and partial density of states of PPy-TDQ. (b) Charge density distribution at VBM and CBM of PPh-TDQ. Band structures are calculated with the PBE-D3 functional, and the band gap calculated with the HSE06 functional is provided in the figure. Spatially separated hole and electron in PPy-TDQ are demonstrated by charge density distribution at VBM and CBM, respectively.

https://doi.org/10.1021/jacsau.2c00169
JACS Au 2022, 2, 1848−1856

the smallest one of 1.00 eV (Figure 3a), which can be ascribed to the low-lying LUMO of TDQ with strong electron-accepting ability (Figure 2b). As illustrated by the charge density distribution of PPy-TDQ in Figure 3b, its VBM is primarily contributed by the PPy node while CBM is mainly localized on the TDQ edge. On the other hand, the energies of VBM and CBM in PPy-TDQ are −5.25 and −4.25 eV, indicating its capability of photocatalytic hydrogen production at pH = 0 (Figure 2a). Moreover, we find that F-substitution on the edge also narrows the band gap and simultaneously lowers the VBM and CBM energies, as demonstrated by PPy-Q and PPy-Q(F), PPy-BT and PPy-BT(F), and PPy-PT and PPy-PT(F), respectively. We ascribe this phenomenon to the strong electron-withdrawing effect of F-substitution, which simultaneously lowers the HOMO and LUMO energies of the edge (Figure 2b). The functional group modification offers a simple yet effective approach to tune the band edge energies of COFs, and it alters the microenvironment of the pore surfaces as well.[58]

The smaller band gaps of these newly designed COFs compared to that of PPy-Ph give rise to the redshift of the absorption spectra (Figure 2c). PPy-Ph exhibits absorption in the range of 300−650 nm covering the visible region of the solar spectrum, which peaks at ∼500 nm as calculated by the G_0W_0-BSE method. Our results are in excellent agreement with the experimental absorption spectrum of PPy-Ph that spans from 360 to 620 nm with the maximum absorption at 497 nm; the calculated optical band gap of 2.14 eV also reproduces well the experimental value of 2.03 eV.[22] The absorption spectra of other COFs are broadened and even extend to 900 nm when the LUMO of the edges becomes lower and lower (Figures 2c and S17). Again, PPy-TDQ shows the broadest absorption spanning from 300 to 900 nm, and it can harvest a wide range of visible and NIR light. Our results demonstrate that the solar light-harvesting ability of these newly designed COFs is superior to g-C_3N_4 and N_3-COF whose band gaps are about 2.7 eV and the absorption spectra fall below 400 and 500 nm, respectively, covering only a small portion of the visible region.[18,59] In addition to the band gap and optical absorption, VBM and CBM energies of COFs are also effectively tuned by chemical building block substitution and modifications to meet the stringent requirement posed by the electrical potential of water splitting. According to Figure 2a, all these PPy-based COFs are capable of HER under the standard condition (pH = 0).

Suppressing the Excitonic Effect in COFs To Foster Electron−Hole Separation

Following the photon absorption, the Coulombic-bound electron−hole pair, namely, the exciton is generated, which subsequently dissociates into free charge carriers to trigger chemical reactions at the electrolyte−photocatalyst interface. The excitonic effect is one of the most essential features that govern the quantum efficiency of photocatalysis. It can be described by the exciton binding energy, which measures the electrostatic interaction within an electron−hole pair. The exciton binding energy is defined as $E_b = E_{elec} - E_{opt}$,[60] where E_{elec} and E_{opt} represent the quasi-particle electric and optical band gaps, respectively.[44] Although the strong interaction within an electron−hole pair has been long recognized for organic photocatalysis,[33] in which E_b is often larger than 1 eV, how to reduce the exciton binding energy and facilitate exciton dissociation remains an open question.

In order to understand the excitonic effect in COFs, we first calculate the exciton binding energy E_b with the G_0W_0-BSE method, a state-of-the-art approach to account for the excitonic effect. As shown in Figures 4a, S18, and Table 1, a positive correlation between E_b and the optical band gap E_{opt} is obviously seen; E_b is substantially reduced as the optical absorption is red-shifted to the NIR region. The exciton binding energy in PPy-Ph (sp^2c-COF) is ∼1200 meV, which is comparable to that in g-C_3N_4,[59] while E_b in PPy-TDQ is 700 meV, nearly half of that in sp^2c-COF and g-C_3N_4. In principle,

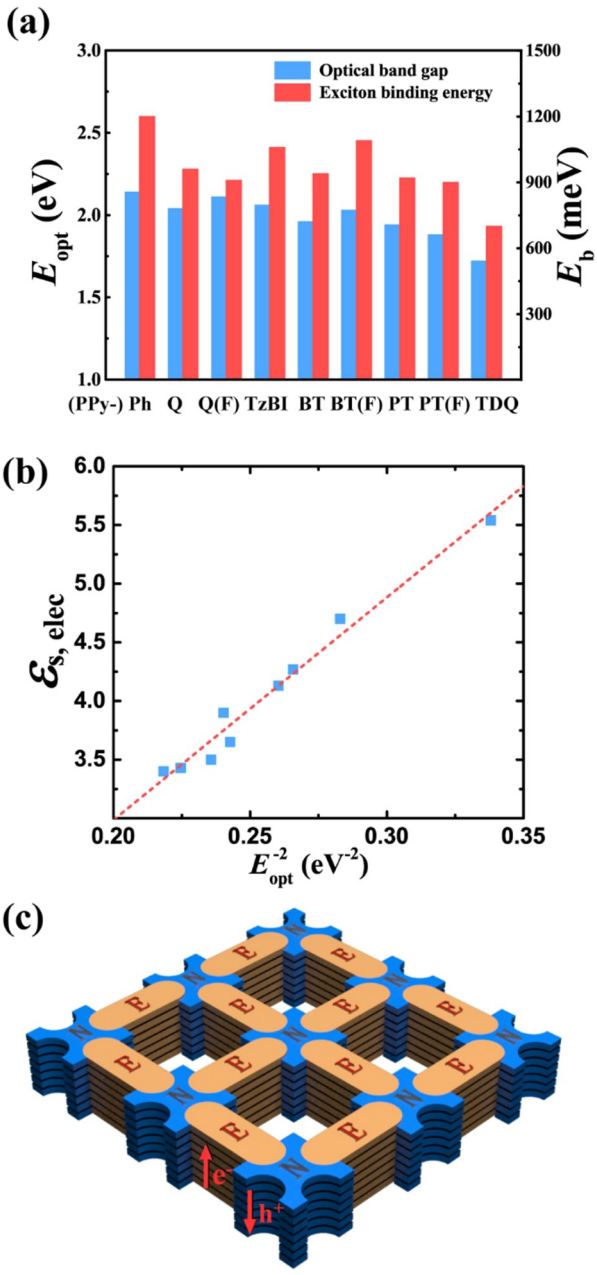

Figure 4. (a) Positive correlation between the optical band gap and the exciton binding energy of COFs. (b) Relationship between the electronic static dielectric constant ($\varepsilon_{s,elec}$) and the optical band gap ($E_{opt} = \hbar\omega_e$) of COFs, well represented by the formula $\varepsilon_{s,elec} = 1 + Ne^2/(m\varepsilon_0\omega_e^2)$. The red dashed line is a linear fit of the data. (c) Schematic illustration of the out-of-plane stacked structure of COFs and the spatial separation of one-dimensional transport channels for electrons and holes, respectively.

https://doi.org/10.1021/jacsau.2c00169
JACS Au 2022, 2, 1848−1856

the exciton binding energy is determined by the reduced mass of exciton (m^*) and the dielectric screening (ε_s).[40] We notice that the reduced mass of exciton barely changes in these COFs (Table 1). The static dielectric constant arises from ionic and electronic contributions and can be written as $\varepsilon_s = \varepsilon_{s,ion} + \varepsilon_{s,elec}$.[61] The ionic response ($\varepsilon_{s,ion}$) is associated with the motion of atoms, which generates an oscillating dipole as with infrared active lattice vibrations, and it is the dominating mechanism in inorganic solids. The electronic response ($\varepsilon_{s,elec}$) accounts for the change of electronic polarizability with the electric field, and it is the dominating mechanism in organic solids, especially in nonpolar materials.[61] As illustrated in Figures 4b and S19, we uncover a linear relationship between the electronic static dielectric $\varepsilon_{s,elec}$ and E^{-2}_{opt} in the series of COFs, so the dielectric screening increases as the optical band gap decreases. These results can be explained with the Lorentz oscillator model, which predicts that the electronic static dielectric ($\varepsilon_{s,elec}$) is related to the optical absorption frequency (ω_e) by $\varepsilon_{s,elec} = 1 + Ne^2/(m\varepsilon_0\omega_e^2)$, where m and N represent the mass and number of oscillators per volume, respectively, and ω_e is the resonance frequency of oscillation, which corresponds to the average electronic excitation energy.[61] Therefore, the exciton binding energy of PPy-TDQ is the smallest since its dielectric constant of 6.05 is the largest (Table 1). The finding that E_b in layer-stacked COFs is governed by ε_s is fundamentally different from that observed in 3D inorganic semiconductors, where the screening effect is so large that the effective mass m^* becomes a dominating factor of E_b; it also differs from 2D inorganic semiconductors where a linear scaling law between E_b and the quasi-particle band gap E_{elec} with $E_b \approx E_{elec}/4$ was established.[62]

All in all, we show that both enhanced solar light harvesting and easier exciton dissociation have been simultaneously realized in COFs with narrow band gaps. Furthermore, we would like to point out that COFs of the Lieb lattice constructed by node units of C_2 or C_4 symmetry, such as PPy, porphyrin, and phthalocyanine, lack a flat band, which usually shows up at CBM or VBM in COFs of the kagome lattice constructed by node units of C_3 symmetry (Figures S20 and S21).[49,63,64] This flat band is formed by nonbonding orbitals and is associated with a heavy electron or hole, and exciton, which will lead to an intriguing magnetic phenomenon but is not desirable for exciton dissociation and high speed charge transport.[63]

These COFs, except for PPy-PT, PPy-PT(F), and PPy-Q, possess an indirect band gap where the VBM and CBM appear at different k-points, so that the photogenerated electron and hole have different momenta. The transition from CBM to VBM thereby requires the change of the electron wavevector, which will further inhibit exciton annihilation and prolong its lifetime,[61] in contrast to COFs with a direct band gap. On the other hand, as illustrated by the partial density distribution in Figures 3b, S3, and S16, the VBM of all COFs, except for PPy-Ph, arises primarily from the node, while CBM arises from the edge, owing to the large energy offset between the HOMOs or LUMOs of nodes and edges. It means that the photogenerated electron−hole pair is spatially separated, which is favorable for exciton dissociation, like that in type-II heterostructures with a staggered band gap. Moreover, nodes and edges stack along the out-of-plane direction, forming a one-dimensional channel for hole and electron transport, respectively.[28] These separated transport channels represent a unique feature of layer-stacked and conjugated COFs, which can enlarge the interface area between the electron and the hole to foster their separation (Figures 4c, S22, and S23).

Photocatalytic Hydrogen Production with High STH Efficiency

To confirm the photocatalytic hydrogen generation activity of these catalysts, we calculate the Gibbs free energy change of HER on PPy-TDQ. Computational details are described in Computational Methods. Various reaction sites on the TDQ moiety are considered because the photogenerated electron is mainly localized on the edge. Although the effective mass of this localized electron is relatively large, the porous nature of COFs allows the HER to take place locally on the pore wall, thus avoiding the long-distance migration of the photoexcited electron. As illustrated by the Gibbs free energy profile of HER under the standard condition (Figure 5a), the overall trend of $\Delta G(H^*)$ is S > C > N. We notice that hydrogen adsorption on the sulfur site shows the highest $\Delta G(H^*)$ because it has to break a σ bond. The carbon site on the cyano group (−CN) also shows high $\Delta G(H^*)$ because hydrogen adsorption on it has to break a C≡N triple bond, whereas the carbon site on

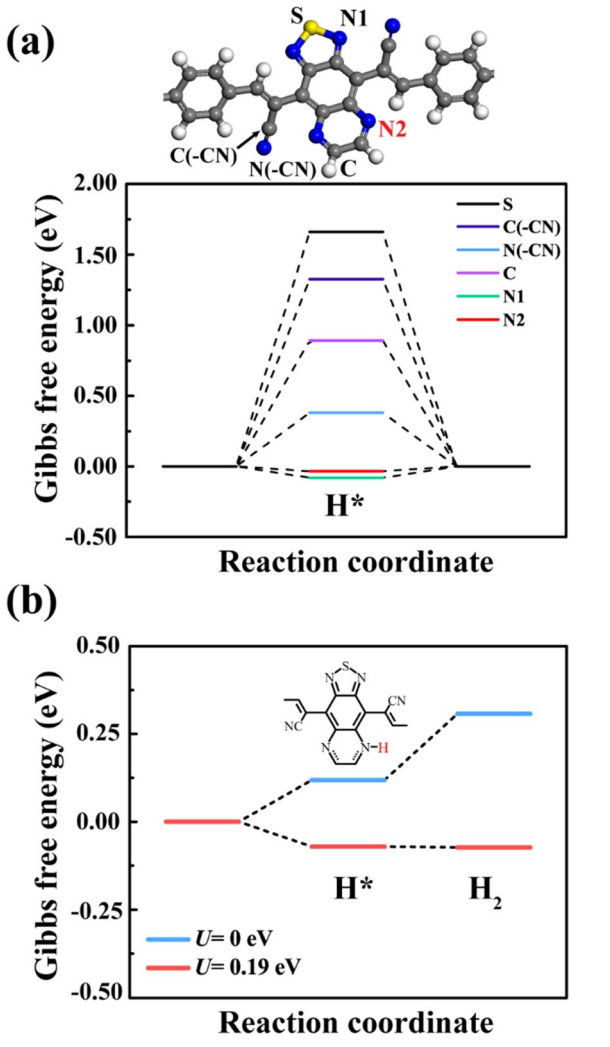

Figure 5. (a) Gibbs free energy changes of HER on various catalytic sites of PPy-TDQ at pH = 0. (b) Gibbs free energy changes of HER on the N2 site of PPy-TDQ at pH = 2.6 (in a 0.1 M ascorbic acid solution), with U = 0 eV (blue) and U = 0.19 eV (red), respectively. The H* structure is shown in the inset.

https://doi.org/10.1021/jacsau.2c00169
JACS Au 2022, 2, 1848−1856

the TDQ edge shows moderate $\Delta G(H^*)$ since hydrogen adsorption on the aromatic carbon only breaks a π bond. The nitrogen site, either on −CN or on TDQ, is more favorable for hydrogen adsorption than the carbon site because formation of an N−H bond gains more energy than the formation of a C−H bond. Among them, the N2 site on the TDQ edge shows the smallest $|\Delta G(H^*)|$ of 0.03 eV, implying its promising catalytic activity for HER. To further validate that the photogenerated electron can indeed drive the reaction in a 0.1 M ascorbic acid solution (pH = 2.6), which is commonly used in photocatalytic experiments with COFs,[40] we calculate the Gibbs free energy change on the N2 site in the presence and absence of light-induced bias potential (U). As shown in Figure 5b, in the dark, this bias potential is zero and each fundamental reaction step is uphill in energy, so it is thermodynamically forbidden. While under sunlight irradiation, the bias potential is 0.19 eV and the reaction becomes downhill in energy, which implies that the N2 site of PPy-TDQ is indeed capable of photocatalytic HER upon visible-to-NIR light irradiation, and an upper limit of STH energy conversion efficiency of 56.6% is predicted. Moreover, PPy-TDQ is also capable of HER at pH = 0 under light irradiation as shown in Figure S24.

CONCLUSIONS

In summary, we demonstrate a facile approach to simultaneously suppress the excitonic effect and enhance the solar light absorption in COFs by a rational molecular design and chemical modifications. The idea of the frontier orbital alignment of molecular building blocks is applied to COFs for tuning their electronic and excitonic properties related to photocatalysis and guiding the design of new photocatalysts with high efficiency. More importantly, we uncover a linear relationship between the electronic static dielectric $\varepsilon_{s,elec}$ and E^{-2}_{opt} in a series of 2D layered COFs of the Lieb lattice and thereby a positive correlation between the exciton binding energy and the optical band gap of COFs. The designed COFs show tunable band gaps from 1.72 down to 1.00 eV, and those with smaller band gaps can harvest a larger portion of sunlight in both visible and NIR regions and at the same time exhibit the suppressed excitonic effect to attain a higher quantum efficiency. Among them, PPy-TDQ exhibits the smallest band gap of 1.00 eV, the broadest light absorption up to 900 nm, and the smallest exciton binding energy of 700 meV, which is nearly half that of g-C_3N_4, a well-recognized organic photocatalyst. Furthermore, we show that PPy-TDQ can facilitate metal-free HER under visible and NIR light irradiation with a very high theoretical STH efficiency. Our study not only provides comprehensive insights and an effective approach to regulate the exciton-related properties of COFs for enhanced quantum efficiency in photocatalytic hydrogen production but also sheds light on their applications in other solar energy conversion techniques.

COMPUTATIONAL METHODS

We performed DFT calculations for all the electronic properties of COFs in this study, including the optimization of lattice constants and atomic coordinates, as implemented in the Vienna ab initio simulation package (VASP 5.3.5)[65] using the projector augmented wave[66] method and the Perdew−Burke−Ernzerhof (PBE)[67] exchange-correlation functional. Grimme's D3 approach was applied to include the London dispersion correction,[68] and the Heyd−Scuseria−Ernzerhof (HSE06)[69] hybrid functional was used to calculate the accurate band gap of COFs. Coordinates of high-symmetry k-points in band structures are provided in Table S3. The electronic and ionic dielectric constants were calculated with the linear response theory and the density functional perturbation theory respectively implemented in VASP 5.3.5. Furthermore, the GW method at the level of G_0W_0 was applied to calculate the quasi-particle band gap and it was combined with the Bethe−Salpeter equation (BSE) to obtain the optical band gap and exciton binding energy. In the lattice parameter optimization, a cutoff energy of 400 eV for the plane-wave basis set was employed, while in the static calculation, a cutoff energy of 600 eV was used. Furthermore, the convergence criterion of forces during the optimization was 0.02 eV $Å^{-1}$. The energy convergence criterion in the self-consistent field iteration was 10^{-5} eV in the optimization while 10^{-6} eV in the static calculation. The partial charge density was plotted by VESTA and the isovalue was set to be 0.002 e $Bohr^{-3}$. A Monkhorst−Pack k-mesh of 1 × 1 × 5 was used in the structural relaxation of COFs, while a denser k-mesh of 1 × 1 × 8 was used to obtain the converged charge density. Other settings were default for VASP. A k-mesh of 1 × 1 × 8 was also used in the G_0W_0-BSE calculation for COFs. As for g-C_3N_4, a k-mesh of 5 × 5 × 5 was used for both structural optimization and G_0W_0-BSE calculation, while a k-mesh of 9 × 9 × 9 was used in the static calculation. The long-range corrected functional ωB97XD and the def2tzvp basis set were used to calculate the frontier orbital energies of molecular building blocks of COFs with the Gaussian16 program package.[70]

As suggested by Nørskov and co-workers,[71] HER can be considered as two one-electron reduction processes:

$$* + H^+ + e^- \rightarrow H^* \quad (1)$$

$$H^* + H^+ + e^- \rightarrow * + H_2 \quad (2)$$

where the photocatalyst is denoted as *, while H* represents the intermediate of the reaction. The Gibbs free energy change of a reaction, ΔG, can be defined as $\Delta G = \Delta E + \Delta ZPE + \Delta_{0\rightarrow 298}H - T\Delta S$, where ΔE, ΔZPE, ΔH, and ΔS are the changes of the self-consistent field energy (E), zero-point vibrational energy (ZPE), thermal energy (H), and entropy (S), respectively. For gaseous species, contributions from the electronic, translational, rotational, and vibrational degrees of freedom were considered. For adsorbed species, only contributions from the electronic and vibrational degrees of freedom were included. We derived thermodynamic corrections with VASPKIT[72] based on the output from VASP. By applying the computational hydrogen electrode model, the Gibbs free energy change of the above reactions can be calculated as

$$\Delta G_1 = G(H^*) - G(*) - 1/2G(H_2) + \Delta pH - U \quad (3)$$

$$\Delta G_2 = 1/2G(H_2) + G(*) - G(H^*) + \Delta pH - U \quad (4)$$

where ΔpH = 0.059 pH, according to Nernst's equation, accounts for the influence of pH in an aqueous solution, while U represents the driving force for the electron, which can be derived from the energy difference between CBM and the standard hydrogen electrode potential (in eV). To model HER, a 1 × 1 × 3 supercell of COFs was constructed, and the hydrogen atom was adsorbed to different sites on the edge unit. A k-mesh of 1 × 1 × 3 was used to optimize the structure of H*. The spin-polarization effect was considered in the calculation of the hydrogen-adsorbed intermediate H*.

The STH conversion efficiency of all the COFs included in Table 1 was calculated using the following equation:

$$STH = \frac{\int_0^{\text{absorption edge}} 1.23\, I(\lambda)\lambda d\lambda}{\int_0^{2000} 1240\, I(\lambda) d\lambda} \times QE \quad (5)$$

where λ represents the light wavelength, 2000 nm is taken as the maximum wavelength of the solar spectrum, QE is the quantum efficiency and is assumed to be 100%, and $I(\lambda)$ stands for the blackbody radiation intensity at 6000 K to simulate the solar spectrum.[30]

https://doi.org/10.1021/jacsau.2c00169
JACS Au 2022, 2, 1848−1856

■ ASSOCIATED CONTENT

Supporting Information

The Supporting Information is available free of charge at https://pubs.acs.org/doi/10.1021/jacsau.2c00169.

Band structures, charge densities, absorption spectra, and optimized structures of PPy-BT(F), PPy-PT, PPy-PT(F), PPy-TDQ, PPy-TzBI, PPy-Q, and PPy-Q(F), and atomic coordinates of molecular building blocks (PDF)

■ AUTHOR INFORMATION

Corresponding Author

Dong Wang − *MOE Key Laboratory of Organic OptoElectronics and Molecular Engineering, Department of Chemistry, Tsinghua University, Beijing 100084, P. R. China;* orcid.org/0000-0002-0594-0515; Email: dong913@mail.tsinghua.edu.cn

Author

Hongde Yu − *MOE Key Laboratory of Organic OptoElectronics and Molecular Engineering, Department of Chemistry, Tsinghua University, Beijing 100084, P. R. China;* orcid.org/0000-0002-2576-271X

Complete contact information is available at: https://pubs.acs.org/10.1021/jacsau.2c00169

Author Contributions

D.W. supervised this study. H.Y. performed theoretical calculations. H.Y. and D.W. discussed the results and cowrote the paper. All authors have given approval to the final version of the manuscript.

Notes

The authors declare no competing financial interest.

■ ACKNOWLEDGMENTS

This work is supported by the National Natural Science Foundation of China (Grant Nos. 22073055 and 21673123). Computational resources are provided by the Tsinghua Supercomputing Center.

■ REFERENCES

(1) Hisatomi, T.; Domen, K. Reaction Systems for Solar Hydrogen Production via Water Splitting with Particulate Semiconductor Photocatalysts. *Nat. Catal.* **2019**, *2*, 387−399.

(2) Kudo, A.; Miseki, Y. Heterogeneous Photocatalyst Materials for Water Splitting. *Chem. Soc. Rev.* **2009**, *38*, 253−278.

(3) Wang, Y.; Suzuki, H.; Xie, J.; Tomita, O.; Martin, D. J.; Higashi, M.; Kong, D.; Abe, R.; Tang, J. Mimicking Natural Photosynthesis: Solar to Renewable H_2 Fuel Synthesis by Z-Scheme Water Splitting Systems. *Chem. Rev.* **2018**, *118*, 5201−5241.

(4) Sivula, K.; van de Krol, R. Semiconducting Materials for Photoelectrochemical Energy Conversion. *Nat. Rev. Mater.* **2016**, *1*, 15010.

(5) Fujishima, A.; Honda, K. Electrochemical Photolysis of Water at a Semiconductor Electrode. *Nature* **1972**, *238*, 37−38.

(6) Chen, S.; Takata, T.; Domen, K. Particulate Photocatalysts for Overall Water Splitting. *Nat. Rev. Mater.* **2017**, *2*, 17050.

(7) Wang, Q.; Hisatomi, T.; Jia, Q.; Tokudome, H.; Zhong, M.; Wang, C.; Pan, Z.; Takata, T.; Nakabayashi, M.; Shibata, N.; Li, Y.; Sharp, I. D.; Kudo, A.; Yamada, T.; Domen, K. Scalable Water Splitting on Particulate Photocatalyst Sheets with a Solar-to-Hydrogen Energy Conversion Efficiency Exceeding 1%. *Nat. Mater.* **2016**, *15*, 611−615.

(8) Wang, X.; Maeda, K.; Thomas, A.; Takanabe, K.; Xin, G.; Carlsson, J. M.; Domen, K.; Antonietti, M. A Metal-Free Polymeric Photocatalyst for Hydrogen Production from Water under Visible Light. *Nat. Mater.* **2009**, *8*, 76−80.

(9) Zhao, D.; Wang, Y.; Dong, C.-L.; Huang, Y.-C.; Chen, J.; Xue, F.; Shen, S.; Guo, L. Boron-Doped Nitrogen-Deficient Carbon Nitride-Based Z-Scheme Heterostructures for Photocatalytic Overall Water Splitting. *Nat. Energy* **2021**, *6*, 388−397.

(10) Sprick, R. S.; Jiang, J.-X.; Bonillo, B.; Ren, S.; Ratvijitvech, T.; Guiglion, P.; Zwijnenburg, M. A.; Adams, D. J.; Cooper, A. I. Tunable Organic Photocatalysts for Visible-Light-Driven Hydrogen Evolution. *J. Am. Chem. Soc.* **2015**, *137*, 3265−3270.

(11) Woods, D. J.; Sprick, R. S.; Smith, C. L.; Cowan, A. J.; Cooper, A. I. A Solution-Processable Polymer Photocatalyst for Hydrogen Evolution from Water. *Adv. Energy Mater.* **2017**, *7*, 1700479.

(12) Sprick, R. S.; Bonillo, B.; Clowes, R.; Guiglion, P.; Brownbill, N. J.; Slater, B. J.; Blanc, F.; Zwijnenburg, M. A.; Adams, D. J.; Cooper, A. I. Visible-Light-Driven Hydrogen Evolution Using Planarized Conjugated Polymer Photocatalysts. *Angew. Chem., Int. Ed.* **2016**, *128*, 1824−1828.

(13) Zhang, G.; Lan, Z. A.; Wang, X. Conjugated Polymers: Catalysts for Photocatalytic Hydrogen Evolution. *Angew. Chem., Int. Ed.* **2016**, *55*, 15712−15727.

(14) Xu, S.; Sun, H.; Addicoat, M.; Biswal, B. P.; He, F.; Park, S.; Paasch, S.; Zhang, T.; Sheng, W.; Brunner, E.; Hou, Y.; Richter, M.; Feng, X. Thiophene-Bridged Donor-Acceptor sp^2-Carbon-Linked 2D Conjugated Polymers as Photocathodes for Water Reduction. *Adv. Mater.* **2021**, *33*, 2006274.

(15) Wang, L.; Zhang, Y.; Chen, L.; Xu, H.; Xiong, Y. 2D Polymers as Emerging Materials for Photocatalytic Overall Water Splitting. *Adv. Mater.* **2018**, *30*, 1801955.

(16) Jing, Y.; Heine, T. Making 2D Topological Polymers a Reality. *Nat. Mater.* **2020**, *19*, 823−824.

(17) Thote, J.; Aiyappa, H. B.; Deshpande, A.; Díaz Díaz, D.; Kurungot, S.; Banerjee, R. A Covalent Organic Framework-Cadmium Sulfide Hybrid as a Prototype Photocatalyst for Visible-Light-Driven Hydrogen Production. *Chem. − Eur. J.* **2014**, *20*, 15961−15965.

(18) Vyas, V. S.; Haase, F.; Stegbauer, L.; Savasci, G.; Podjaski, F.; Ochsenfeld, C.; Lotsch, B. V. A Tunable Azine Covalent Organic Framework Platform for Visible Light-Induced Hydrogen Generation. *Nat. Commun.* **2015**, *6*, 8508.

(19) Sick, T.; Hufnagel, A. G.; Kampmann, J.; Kondofersky, I.; Calik, M.; Rotter, J. M.; Evans, A.; Döblinger, M.; Herbert, S.; Peters, K.; Böhm, D.; Knochel, P.; Medina, D. D.; Fattakhova-Rohlfing, D.; Bein, T. Oriented Films of Conjugated 2D Covalent Organic Frameworks as Photocathodes for Water Splitting. *J. Am. Chem. Soc.* **2018**, *140*, 2085−2092.

(20) Banerjee, T.; Gottschling, K.; Savasci, G.; Ochsenfeld, C.; Lotsch, B. V. H_2 Evolution with Covalent Organic Framework Photocatalysts. *ACS Energy Lett.* **2018**, *3*, 400−409.

(21) Wang, X.; Chen, L.; Chong, S. Y.; Little, M. A.; Wu, Y.; Zhu, W.-H.; Clowes, R.; Yan, Y.; Zwijnenburg, M. A.; Sprick, R. S.; Cooper, A. I. Sulfone-Containing Covalent Organic Frameworks for Photocatalytic Hydrogen Evolution from Water. *Nat. Chem.* **2018**, *10*, 1180−1189.

(22) Jin, E.; Lan, Z.; Jiang, Q.; Geng, K.; Li, G.; Wang, X.; Jiang, D. 2D sp^2 Carbon-Conjugated Covalent Organic Frameworks for Photocatalytic Hydrogen Production from Water. *Chem* **2019**, *5*, 1632−1647.

(23) Pachfule, P.; Acharjya, A.; Roeser, J.; Langenhahn, T.; Schwarze, M.; Schomäcker, R.; Thomas, A.; Schmidt, J. Diacetylene Functionalized Covalent Organic Framework (COF) for Photocatalytic Hydrogen Generation. *J. Am. Chem. Soc.* **2018**, *140*, 1423−1427.

(24) Stegbauer, L.; Zech, S.; Savasci, G.; Banerjee, T.; Podjaski, F.; Schwinghammer, K.; Ochsenfeld, C.; Lotsch, B. V. Tailor-Made Photoconductive Pyrene-Based Covalent Organic Frameworks for

Visible-Light Driven Hydrogen Generation. *Adv. Energy Mater.* **2018**, *8*, 1703278.
(25) Waller, P. J.; Gándara, F.; Yaghi, O. M. Chemistry of Covalent Organic Frameworks. *Acc. Chem. Res.* **2015**, *48*, 3053−3063.
(26) Cote, A. P.; Benin, A. I.; Ockwig, N. W.; O'Keeffe, M.; Matzger, A. J.; Yaghi, O. M. Porous, Crystalline, Covalent Organic Frameworks. *Science* **2005**, *310*, 1166−1170.
(27) Li, X.; Yadav, P.; Loh, K. P. Function-Oriented Synthesis of Two-Dimensional (2D) Covalent Organic Frameworks from 3D Solids to 2D Sheets. *Chem. Soc. Rev.* **2020**, *49*, 4835−4866.
(28) Chen, X.; Geng, K.; Liu, R.; Tan, K. T.; Gong, Y.; Li, Z.; Tao, S.; Jiang, Q.; Jiang, D. Covalent Organic Frameworks: Chemical Approaches to Designer Structures and Built-In Functions. *Angew. Chem., Int. Ed.* **2020**, *59*, 5050−5091.
(29) Huang, N.; Wang, P.; Jiang, D. Covalent Organic Frameworks: A Materials Platform for Structural and Functional Designs. *Nat. Rev. Mater.* **2016**, *1*, 16068.
(30) Wan, Y.; Wang, L.; Xu, H.; Wu, X.; Yang, J. A Simple Molecular Design Strategy for Two-Dimensional Covalent Organic Framework Capable of Visible-Light-Driven Water Splitting. *J. Am. Chem. Soc.* **2020**, *142*, 4508−4516.
(31) Jing, Y.; Zhou, Z.; Geng, W.; Zhu, X.; Heine, T. 2D Honeycomb-Kagome Polymer Tandem as Effective Metal-Free Photocatalysts for Water Splitting. *Adv. Mater.* **2021**, *33*, 2008645.
(32) Zhou, Z.; Springer, M. A.; Geng, W.; Zhu, X.; Li, T.; Li, M.; Jing, Y.; Heine, T. Rational Design of Two-Dimensional Binary Polymers from Heterotriangulenes for Photocatalytic Water Splitting. *J. Phys. Chem. Lett.* **2021**, *12*, 8134−8140.
(33) Ghosh, S.; Nakada, A.; Springer, M. A.; Kawaguchi, T.; Suzuki, K.; Kaji, H.; Baburin, I.; Kuc, A.; Heine, T.; Suzuki, H.; Abe, R.; Seki, S. Identification of Prime Factors to Maximize the Photocatalytic Hydrogen Evolution of Covalent Organic Frameworks. *J. Am. Chem. Soc.* **2020**, *142*, 9752−9762.
(34) Gottschling, K.; Savasci, G.; Vignolo-González, H.; Schmidt, S.; Mauker, P.; Banerjee, T.; Rovó, P.; Ochsenfeld, C.; Lotsch, B. V. K. Rational Design of Covalent Cobaloxime-Covalent Organic Framework Hybrids for Enhanced Photocatalytic Hydrogen Evolution. *J. Am. Chem. Soc.* **2020**, *142*, 12146−12156.
(35) Chen, W.; Wang, L.; Mo, D.; He, F.; Wen, Z.; Wu, X.; Xu, H.; Chen, L. Modulating Benzothiadiazole-Based Covalent Organic Frameworks via Halogenation for Enhanced Photocatalytic Water Splitting. *Angew. Chem., Int. Ed.* **2020**, *59*, 16902−16909.
(36) Wei, S.; Zhang, F.; Zhang, W.; Qiang, P.; Yu, K.; Fu, X.; Wu, D.; Bi, S.; Zhang, F. Semiconducting 2D Triazine-Cored Covalent Organic Frameworks with Unsubstituted Olefin Linkages. *J. Am. Chem. Soc.* **2019**, *141*, 14272−14279.
(37) Rahman, M. Z.; Kibria, M. G.; Mullins, C. B. Metal-Free Photocatalysts for Hydrogen Evolution. *Chem. Soc. Rev.* **2020**, *49*, 1887−1931.
(38) Liu, J.; Liu, Y.; Liu, N.; Han, Y.; Zhang, X.; Huang, H.; Lifshitz, Y.; Lee, S.-T.; Zhong, J.; Kang, Z. Metal-Free Efficient Photocatalyst for Stable Visible Water Splitting via a Two-Electron Pathway. *Science* **2015**, *347*, 970−974.
(39) Axelsson, M.; Marchiori, C. F. N.; Huang, P.; Araujo, C. M.; Tian, H. Small Organic Molecule Based on Benzothiadiazole for Electrocatalytic Hydrogen Production. *J. Am. Chem. Soc.* **2021**, *143*, 21229−21233.
(40) Wang, X.; Chen, L.; Chong, S. Y.; Little, M. A.; Wu, Y.; Zhu, W.-H.; Clowes, R.; Yan, Y.; Zwijnenburg, M. A.; Sprick, R. S.; Cooper, A. I. Sulfone-Containing Covalent Organic Frameworks for Photocatalytic Hydrogen Evolution from Water. *Nat. Chem.* **2018**, *10*, 1180−1189.
(41) Flanders, N. C.; Kirschner, M. S.; Kim, P.; Fauvell, T. J.; Evans, A. M.; Helweh, W.; Spencer, A. P.; Schaller, R. D.; Dichtel, W. R.; Chen, L. X. Large Exciton Diffusion Coefficients in Two-Dimensional Covalent Organic Frameworks with Different Domain Sizes Revealed by Ultrafast Exciton Dynamics. *J. Am. Chem. Soc.* **2020**, *142*, 14957−14965.
(42) Qian, Y.; Li, D.; Han, Y.; Jiang, H.-L. Photocatalytic Molecular Oxygen Activation by Regulating Excitonic Effects in Covalent Organic Frameworks. *J. Am. Chem. Soc.* **2020**, *142*, 20763−20771.
(43) Wang, H.; Jin, S.; Zhang, X.; Xie, Y. Excitonic Effects in Polymeric Photocatalysts. *Angew. Chem., Int. Ed.* **2020**, *132*, 23024−23035.
(44) Wang, H.; Liu, W.; He, X.; Zhang, P.; Zhang, X.; Xie, Y. An Excitonic Perspective on Low-Dimensional Semiconductors for Photocatalysis. *J. Am. Chem. Soc.* **2020**, *142*, 14007−14022.
(45) Li, S.; Li, L.; Li, Y.; Dai, L.; Liu, C.; Liu, Y.; Li, J.; Lv, J.; Li, P.; Wang, B. Fully Conjugated Donor-Acceptor Covalent Organic Frameworks for Photocatalytic Oxidative Amine Coupling and Thioamide Cyclization. *ACS Catal.* **2020**, *10*, 8717−8726.
(46) Chen, R.; Shi, J. L.; Ma, Y.; Lin, G.; Lang, X.; Wang, C. Designed Synthesis of a 2D Porphyrin-Based sp^2 Carbon-Conjugated Covalent Organic Framework for Heterogeneous Photocatalysis. *Angew. Chem., Int. Ed.* **2019**, *58*, 6430−6434.
(47) Cheng, P.; Yang, Y. Narrowing the Band Gap: The Key to High-Performance Organic Photovoltaics. *Acc. Chem. Res.* **2020**, *53*, 1218−1228.
(48) Stegbauer, L.; Schwinghammer, K.; Lotsch, B. V. A Hydrazone-Based Covalent Organic Framework for Photocatalytic Hydrogen Production. *Chem. Sci.* **2014**, *5*, 2789−2793.
(49) Springer, M. A.; Liu, T.-J.; Kuc, A.; Heine, T. Topological Two-Dimensional Polymers. *Chem. Soc. Rev.* **2020**, *49*, 2007−2019.
(50) Jiang, W.; Huang, H.; Liu, F. A Lieb-Like Lattice in a Covalent-Organic Framework and Its Stoner Ferromagnetism. *Nat. Commun.* **2019**, *10*, 2207.
(51) Wang, M.; Wang, M.; Lin, H.-H.; Ballabio, M.; Zhong, H.; Bonn, M.; Zhou, S.; Heine, T.; Cánovas, E.; Dong, R.; Feng, X. High-Mobility Semiconducting Two-Dimensional Conjugated Covalent Organic Frameworks with P-Type Doping. *J. Am. Chem. Soc.* **2020**, *142*, 21622−21627.
(52) Ghosh, S.; Tsutsui, Y.; Suzuki, K.; Kaji, H.; Honjo, K.; Uemura, T.; Seki, S. Impact of the Position of the Imine Linker on the Optoelectronic Performance of π-Conjugated Organic Frameworks. *Mol. Syst. Des. Eng.* **2019**, *4*, 325−331.
(53) Zhuang, X.; Zhao, W.; Zhang, F.; Cao, Y.; Liu, F.; Bi, S.; Feng, X. A Two-Dimensional Conjugated Polymer Framework with Fully sp^2-Bonded Carbon Skeleton. *Polym. Chem.* **2016**, *7*, 4176−4181.
(54) Chen, R.; Wang, Y.; Ma, Y.; Mal, A.; Gao, X.-Y.; Gao, L.; Qiao, L.; Li, X.-B.; Wu, L.-Z.; Wang, C. Rational Design of Isostructural 2D Porphyrin-Based Covalent Organic Frameworks for Tunable Photocatalytic Hydrogen Evolution. *Nat. Commun.* **2021**, *12*, 1354.
(55) Pastoetter, D. L.; Xu, S.; Borrelli, M.; Addicoat, M.; Biswal, B. P.; Paasch, S.; Dianat, A.; Thomas, H.; Berger, R.; Reineke, S.; Brunner, E.; Cuniberti, G.; Richter, M.; Feng, X. Synthesis of Vinylene-Linked Two-Dimensional Conjugated Polymers via the Horner-Wadsworth-Emmons Reaction. *Angew. Chem., Int. Ed.* **2020**, *59*, 23620−23625.
(56) Pandey, L.; Risko, C.; Norton, J. E.; Brédas, J.-L. Donor-Acceptor Copolymers of Relevance for Organic Photovoltaics: A Theoretical Investigation of the Impact of Chemical Structure Modifications on the Electronic and Optical Properties. *Macromolecules* **2012**, *45*, 6405−6414.
(57) Yu, H.; Wang, D. Metal-Free Magnetism in Chemically Doped Covalent Organic Frameworks. *J. Am. Chem. Soc.* **2020**, *142*, 11013−11021.
(58) Nagai, A.; Guo, Z.; Feng, X.; Jin, S.; Chen, X.; Ding, X.; Jiang, D. Pore Surface Engineering in Covalent Organic Frameworks. *Nat. Commun.* **2011**, *2*, 536.
(59) Wei, W.; Jacob, T. Strong Excitonic Effects in the Optical Properties of Graphitic Carbon Nitride g-C_3N_4 from First Principles. *Phys. Rev. B* **2013**, *87*, 085202.
(60) Brédas, J.-L. Mind the Gap! *Mater. Horiz.* **2014**, *1*, 17−19.
(61) Cox, P. A. *The Electronic Structure and Chemistry of Solids*; Oxford University Press: 1987.

https://doi.org/10.1021/jacsau.2c00169
JACS Au 2022, 2, 1848−1856

(62) Jiang, Z.; Liu, Z.; Li, Y.; Duan, W. Scaling Universality between Band Gap and Exciton Binding Energy of Two-Dimensional Semiconductors. *Phys. Rev. Lett.* **2017**, *118*, 266401.
(63) Thomas, S.; Li, H.; Zhong, C.; Matsumoto, M.; Dichtel, W. R.; Brédas, J.-L. Electronic Structure of Two-Dimensional π-Conjugated Covalent Organic Frameworks. *Chem. Mater.* **2019**, *31*, 3051−3065.
(64) Ghosh, S.; Tsutsui, Y.; Kawaguchi, T.; Matsuda, W.; Nagano, S.; Suzuki, K.; Kaji, H.; Seki, S. Band-Like Transport of Charge Carriers in Oriented Two-Dimensional Conjugated Covalent Organic Frameworks. *Chem. Mater.* **2022**, *34*, 736−745.
(65) Kresse, G.; Furthmüller, J. Efficient Iterative Schemes for Ab Initio Total-Energy Calculations Using a Plane-Wave Basis Set. *Phys. Rev. B* **1996**, *54*, 11169.
(66) Blöchl, P. E. Projector Augmented-Wave Method. *Phys. Rev. B* **1994**, *50*, 17953.
(67) Perdew, J. P.; Burke, K.; Ernzerhof, M. Generalized Gradient Approximation Made Simple. *Phys. Rev. Lett.* **1996**, *77*, 3865.
(68) Grimme, S.; Antony, J.; Ehrlich, S.; Krieg, H. A Consistent and Accurate Ab Initio Parametrization of Density Functional Dispersion Correction (DFT-D) for the 94 Elements H-Pu. *J. Chem. Phys.* **2010**, *132*, 154104.
(69) Heyd, J.; Scuseria, G. E.; Ernzerhof, M. Hybrid Functionals Based on a Screened Coulomb Potential. *J. Chem. Phys.* **2003**, *118*, 8207−8215.
(70) Frisch, M. J.; Trucks, G. W.; Schlegel, H. B.; Scuseria, G. E.; Robb, M. A.; Cheeseman, J. R.; Scalmani, G.; Barone, V.; Petersson, G. A.; Nakatsuji, H.; Li, X.; Caricato, M.; Marenich, A. V.; Bloino, J.; Janesko, B. G.; Gomperts, R.; Mennucci, B.; Hratchian, H. P.; Ortiz, J. V.; Izmaylov, A. F.; Sonnenberg, J. L.; Williams; Ding, F.; Lipparini, F.; Egidi, F.; Goings, J.; Peng, B.; Petrone, A.; Henderson, T.; Ranasinghe, D.; Zakrzewski, V. G.; Gao, J.; Rega, N.; Zheng, G.; Liang, W.; Hada, M.; Ehara, M.; Toyota, K.; Fukuda, R.; Hasegawa, J.; Ishida, M.; Nakajima, T.; Honda, Y.; Kitao, O.; Nakai, H.; Vreven, T.; Throssell, K.; Montgomery, Jr., J. A.; Peralta, J. E.; Ogliaro, F.; Bearpark, M. J.; Heyd, J. J.; Brothers, E. N.; Kudin, K. N.; Staroverov, V. N.; Keith, T. A.; Kobayashi, R.; Normand, J.; Raghavachari, K.; Rendell, A. P.; Burant, J. C.; Iyengar, S. S.; Tomasi, J.; Cossi, M.; Millam, J. M.; Klene, M.; Adamo, C.; Cammi, R.; Ochterski, J. W.; Martin, R. L.; Morokuma, K.; Farkas, O.; Foresman, J. B.; Fox, D. J. *Gaussian 16 Rev. C.01*; Gaussian Inc.: Wallingford, CT, 2016.
(71) Nørskov, J. K.; Bligaard, T.; Logadottir, A.; Kitchin, J.; Chen, J. G.; Pandelov, S.; Stimming, U. Trends in the Exchange Current for Hydrogen Evolution. *J. Electrochem. Soc.* **2005**, *152*, J23−J26.
(72) Wang, V.; Xu, N.; Liu, J.-C.; Tang, G.; Geng, W.-T. VASPKIT: A User-Friendly Interface Facilitating High-Throughput Computing and Analysis Using Vasp Code. *Comput. Phys. Commun.* **2021**, *267*, 108033.

https://doi.org/10.1021/jacsau.2c00169
JACS Au 2022, 2, 1848−1856